Int. J. Electrochem. Sci., 7 **(2012)** 6365 - 6377

International Journal of
ELECTROCHEMICAL
SCIENCE
www.electrochemsci.org

Formation of Nanoporous Copper with Hybrid-Modal Pore Size Distributions Related to Surface Diffusion of Copper Atoms During Dealloying of Mg 13.5 at.% Cu Alloy in an Acidic Solution

Wenbo Liu[1,2,*], *Shichao Zhang*[1,*], *Ning Li*[2], *Jiwei Zheng*[1], *Shenshen An*[1] *and Yalan Xing*[1]

[1] School of Materials Science and Engineering, Beihang University, Beijing 100191, China
[2] School of Manufacturing Science and Engineering, Sichuan University, Chengdu 610065, China
[*]E-mail: liuwenbo_8338@163.com, csc@buaa.edu.cn

Received: 6 June 2012 / *Accepted:* 19 June 2012 / *Published:* 1 July 2012

Nanoporous copper (NPC) ribbons with hybrid-modal pore size distributions can be facilely fabricated by effectively controlling the surface diffusivity of Cu atoms during chemical dealloying of dual-phase Mg 13.5 at.% Cu alloy with quasieutectic structures in the HCl solution. These NPC ribbons can be featured by a combination of ligament-pore structures with unimodal pore size distributions at superficial layers and those with bimodal pore size distributions in the interior composed of interconnected large-sized pores with highly porous pore walls. All pores in the ligament-pore structures with unimodal and bimodal pore size distributions are 3D, open and bicontinuous. The formation of the novel NPC ribbons can be well explained as a consequence of the greater diffusivity of Cu atoms at the superficial layers induced by the higher absorbed Cl^- concentration. According to the ligament sizes, the surface diffusivity of Cu atoms at the superficial layers can be evaluated as 1.68×10^{-16} m^2 s^{-1}, which is two orders of magnitude greater than that in the interior of the NPC ribbons (3.55×10^{-19} m^2 s^{-1}).

Keywords: Nanoporous copper; Dealloying; One-pot route; Surface diffusivity; Hybrid-modal pore size distribution

1. INTRODUCTION

Nanoporous metals (NPMs), as novel functional materials, have recently attracted considerable interest in a wide variety of applications including catalysis, sensors, actuators, fuel cells, microfluidic flow controllers, and so forth [1-4]. Since it has been found that chemical/electrochemical dealloying can be used to yield a broad range of porous metals, during the latest decades, a great deal of effort has

been directed towards the investigation of NPMs prepared through dealloying [5-8]. Currently, investigations of NPMs have been mainly focused on synthesis. Typically, methods to fabricate porous metals with controlled pore sizes result in synthesis of materials with unimodal pore size distributions. Obviously, the properties of NPMs with multimodal pore size distributions can be optimized through adjusting the pore size and distribution. For instance, for microfluidic-based sensors, a bimodal pore size distribution is desirable in order to achieve fast response time and high sensitivity, in which large-sized pores are useful in microfluidic flow control, while small-sized pores are useful for increasing device surface area as required for sensor applications [9].

It is well-known that the more complex the porous structure of NPMs, the more difficult the synthesis process. Typically, Ding et al. [9] have reported on a two-step dealloying strategy to make free-standing noble metal membranes with a bimodal pore size distribution by performing a annealing/redealloying cycle on Ag-plated nanoporous gold (NPG). However, the cycle prolongs the production time and increases the cost. Zhang and co-workers [10-11] developed a one-pot dealloying route to synthesize the NPMs with bimodal channel size distributions, in which large-sized channels resulting from entire dissolution of solid solutions while small-sized those deriving from part corrosion of intermetallics. However, it is obvious that those large-sized channels cannot be regarded as 3D, open, bicontinuous pores and, to some extent, more like cracks. Recently, our group developed a facile one-pot route to fabricate the NPC with bimodal pore size distributions through rapid solidification and chemical dealloying of dual-phase Al-Cu alloys with quasieutectic structures, which is characteristic of an ideal two-phase bicontinuous microstructure [12]. Obviously, compared to the previous two-step strategy, one-pot route possesses evident advantages of simple processing, economy, and is applicable for large-scale synthesis. Thus, further developing facile preparation methods of NPMs with complex porous structures are crucial for their wide applications, which urgently need to be investigated.

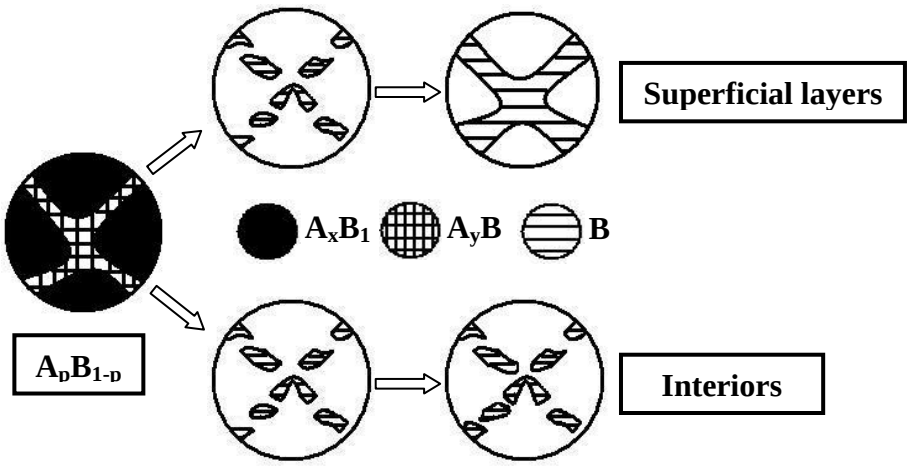

Scheme 1. Schematic diagram showing a typical morphological evolution of a dual-phase alloy with quasieutectic structure through controlling the diffusion kinetics process of MN atoms during dealloying (A_pB_{1-p} is a typical dual-phase alloy with quasieutectic structure, where a relatively large difference exists in the metal/metal-ion equilibrium potentials between A and B, and element A is more electroactive. A_xB_{1-x} and A_yB_{1-y} ($x>y$) denote as the two phases existing in the A_pB_{1-p} alloy. B is the MN element in this case.).

It is generally recognized that the evolution of porous structure during dealloying involves etching of less noble (LN) elements coupled with coarsening of more noble (MN) elements by surface diffusion. Surface diffusion of MN elements along alloy/solution interfaces will play a key role in the formation of NPMs and has a significant influence on length scales of ligaments/pores [5,13]. In our previous work, it has been found that the surface diffusivity of MN atoms along the thickness direction of NPMs during dealloying is markedly different, in which the greater diffusivity often occurs on the surfaces [14]. Inspired by it, it is easy to consider that for dual-phase alloys with quasieutectic structures, further tailoring of length scales and distribution patterns of ligaments/pores along the thickness direction of NPMs could be achieved through effectively controlling the diffusion kinetics process of MN atoms during dealloying, as illustrated in Scheme 1. From this perspective, Mg 13.5 at.% Cu alloy (eutectic point composition: 14.5 at.% Cu) was taken as an example to synthesize the NPC ribbons with hybrid-modal pore size distributions through rapid solidification and one-pot chemical dealloying. The results show that the as-made NPC ribbons can be featured by a combination of ligament-pore structures with unimodal pore size distributions at superficial layers and those with bimodal pore size distributions in the interior composed of interconnected large-sized pores with highly porous pore walls. All pores in the ligament-pore structures with unimodal and bimodal pore size distributions are 3D, open and bicontinuous. In the meantime, the formation mechanism of the novel NPC ribbons is discussed in detail.

2. EXPERIMENTAL SECTION

Mg-Cu alloy with nominal composition of 13.5 at.% Cu was prepared from pure Mg (99.9 wt.%) and pure Cu (99.999 wt.%). Voltaic arc heating was employed to melt the charges in a copper crucible under an argon atmosphere, and then the melt was cooled down into ingots in situ. By use of a single roller melt spinning apparatus, the Mg-Cu ingots were remelted in a quartz tube by high-frequency induction heating and then melt-spun onto a copper roller at a circumferential speed of ~3000 rpm in a controlled argon atmosphere. The obtained alloy ribbons were typically 10-30 μm in thickness, 4-6 mm in width, and several centimeters in length. The rapidly solidified (RS) Mg-Cu alloy ribbons were dealloyed in a 1 wt.% HCl aqueous solution at room temperature (RT) for different times. After dealloying, the samples were rinsed with distilled water and dehydrated alcohol. The as-dealloyed samples were kept in a vacuum chamber to avoid oxidation. Microstructural characterization and analysis of the RS Mg-Cu ribbons and as-dealloyed samples were made using X-ray diffraction (XRD, Rigaku D/Max-2400) with Cu Kα radiation, scanning electron microscopy (FESEM, Hitachi S-4800) with an energy dispersive X-ray (EDX) analyzer, transmission electron microscopy (TEM, JEOL JEM 2100F) with selected-area electron diffraction (SAED), and high-resolution transmission electron microscopy (HRTEM, JEOL JEM 2100F). To test the electrochemical activities of α-Mg and Mg_2Cu phases in the RS Mg-Cu alloy, potentiodynamic polarizations studies were conducted on single-phase α-Mg solid solution and Mg_2Cu intermetallic compound (corresponding to Mg-Cu alloy with a trace amount of Cu and Mg 33 at.% Cu alloy prepared by the same procedure described above) in the HCl solution at RT by using an electrochemical measurement unit (PARSTAT 2273). The

experiments were carried out in a standard three-electrode electrochemical cell (200mL) with a Pt plate electrode as a counter electrode, a saturated calomel electrode (SCE) as a reference electrode, and the alloy ribbon as the working electrode. Polarization scan was performed towards positive values at a scan rate of 1.0 mV s^{-1}, after allowing a steady state potential to develop. In order to evaluate specific surface areas of these as-dealloyed samples, the N_2 adsorption/desorption experiments were carried out at 77 K on a Nova Station A automatic surface area and pore radius distribution apparatus.

3. RESULTS AND DISCUSSION

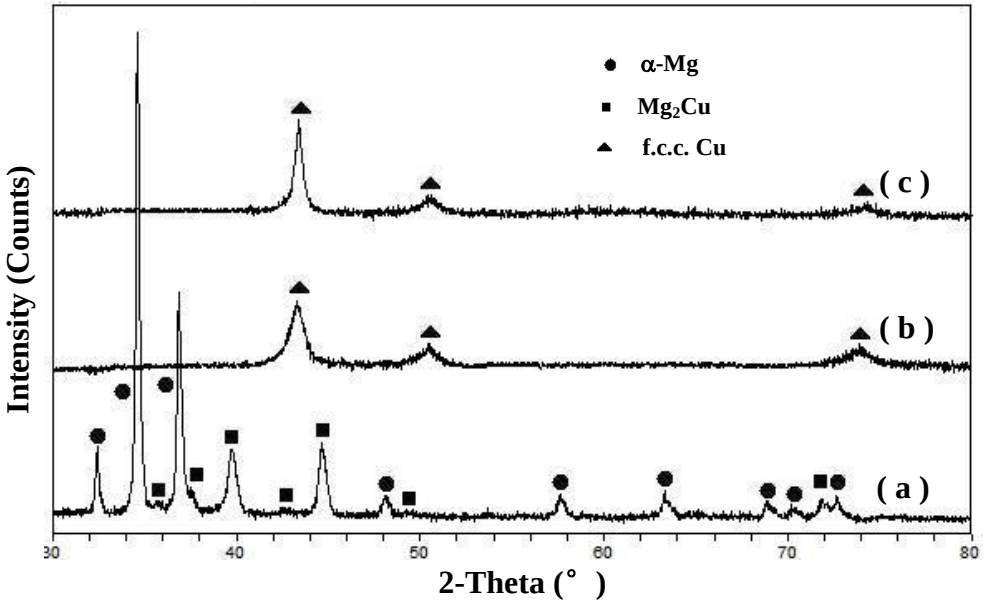

Figure 1. XRD patterns of RS Mg 13.5 at.% Cu alloy ribbon (a) before and (b-d) upon dealloying in the 1 wt.% HCl solution at RT for 5 min, 10 min.

Figure 1 shows the XRD patterns of the RS initial Mg 13.5 at.% Cu alloy ribbons and their as-dealloyed samples upon dealloying in the 1 wt.% HCl solution at RT for different times. The filled circles, squares and triangles in Figure 1 stand for α-Mg, Mg_2Cu and Cu, respectively. As can be seen from part a of Figure 1, the Mg 13.5 at.% Cu alloy is composed of two phases: α-Mg and Mg_2Cu, and the amount of α-Mg is slightly more than that of Mg_2Cu in the alloy. Upon the dealloying over 5 min in the HCl solution, only a face-centered cubic (f.c.c.) Cu phase can be identified in the as-dealloyed samples (parts b and c of Figure 1). It should be noted that the peak width of $(111)_{Cu}$, $(200)_{Cu}$, $(220)_{Cu}$ reflections of the NPC by dealloying in the acidic solution for 5 min is slightly broad compared to that by dealloying for 10 min, suggesting that the length scales of porous structure in the NPC ribbons by dealloying for 5 min are relatively smaller.

Figure 2 shows the typical plane-view and section-view SEM images of the NPC ribbons with bimodal pore size distributions by dealloying of RS Mg 13.5 at.% Cu alloy in the 1 wt.% HCl solution for 5 min. Clearly, the surface exhibits a porous structure with slightly larger pore sizes of ~100 nm as

compared with that of ligament dimensions (50-70 nm, part a of Figure 2). The SEM image at a higher magnification shows the pore walls exhibit an open, bicontinuous interpenetrating ligament-pore structure with length scales of 10-20 nm (part b of Figure 2).

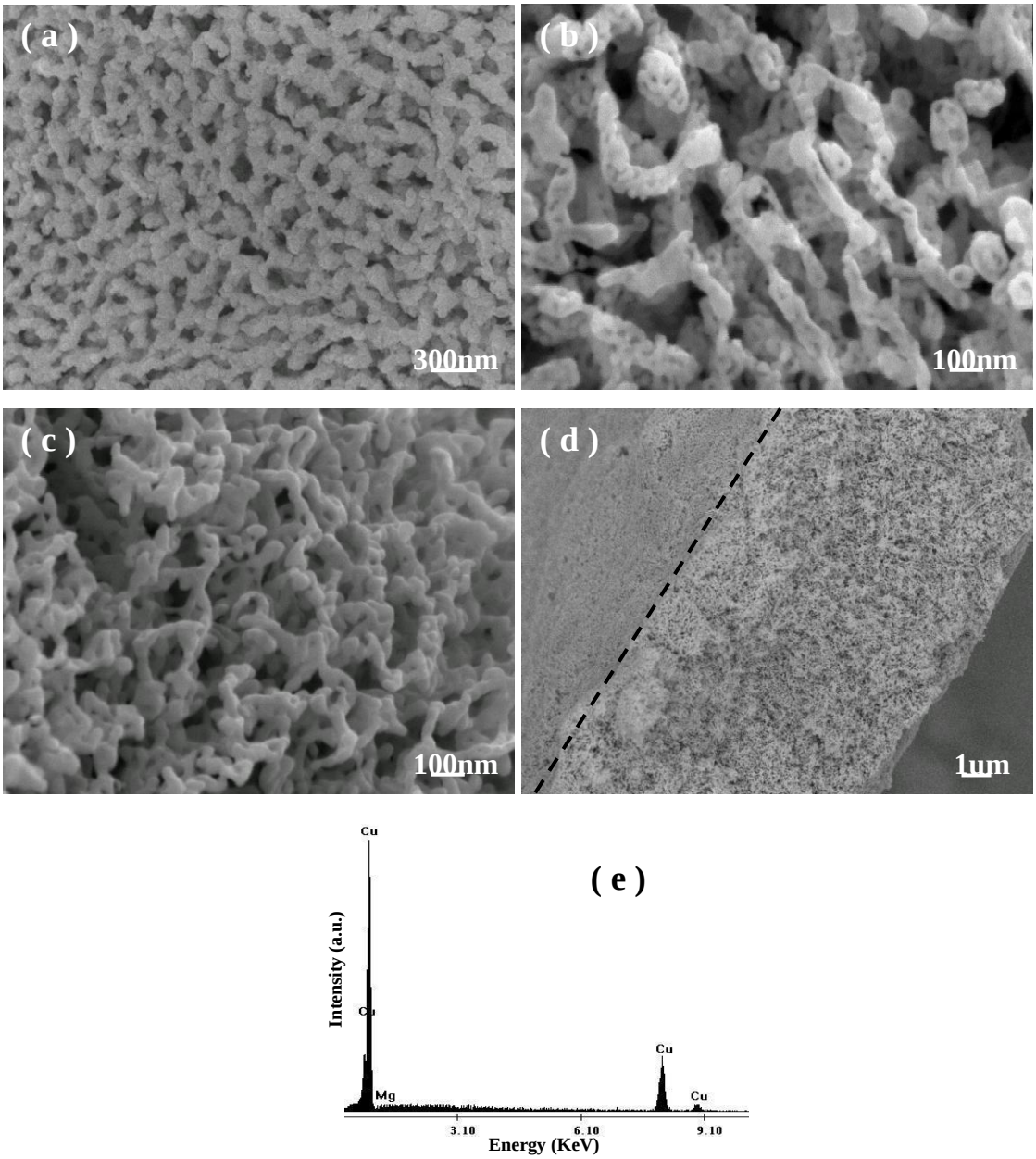

Figure 2. SEM images showing the microstructure of the NPC with bimodal pore size distributions by dealloying in the 1 wt.% HCl solution for 5 min. Parts a and b are the plane views; parts c and d are the section views. Part b shows the plane-view SEM image at a higher magnification; part d shows the entire section-view SEM image at a lower magnification, in which broken line denotes the edge between surface and section. (e) A typical EDX spectrum shows the composition of NPC by dealloying for 5 min. a.u.: arbitrary units.

Moreover, the section view of the NPC ribbons clearly shows, in the inner space of it, the large-sized pores continuously penetrate the whole ribbons, and the large-sized pore walls also possess

an open, bicontinuous interpenetrating ligament-pore structure, suggesting that the nanoporous structure of the pore walls is 3D (parts c and d of Figure 2).

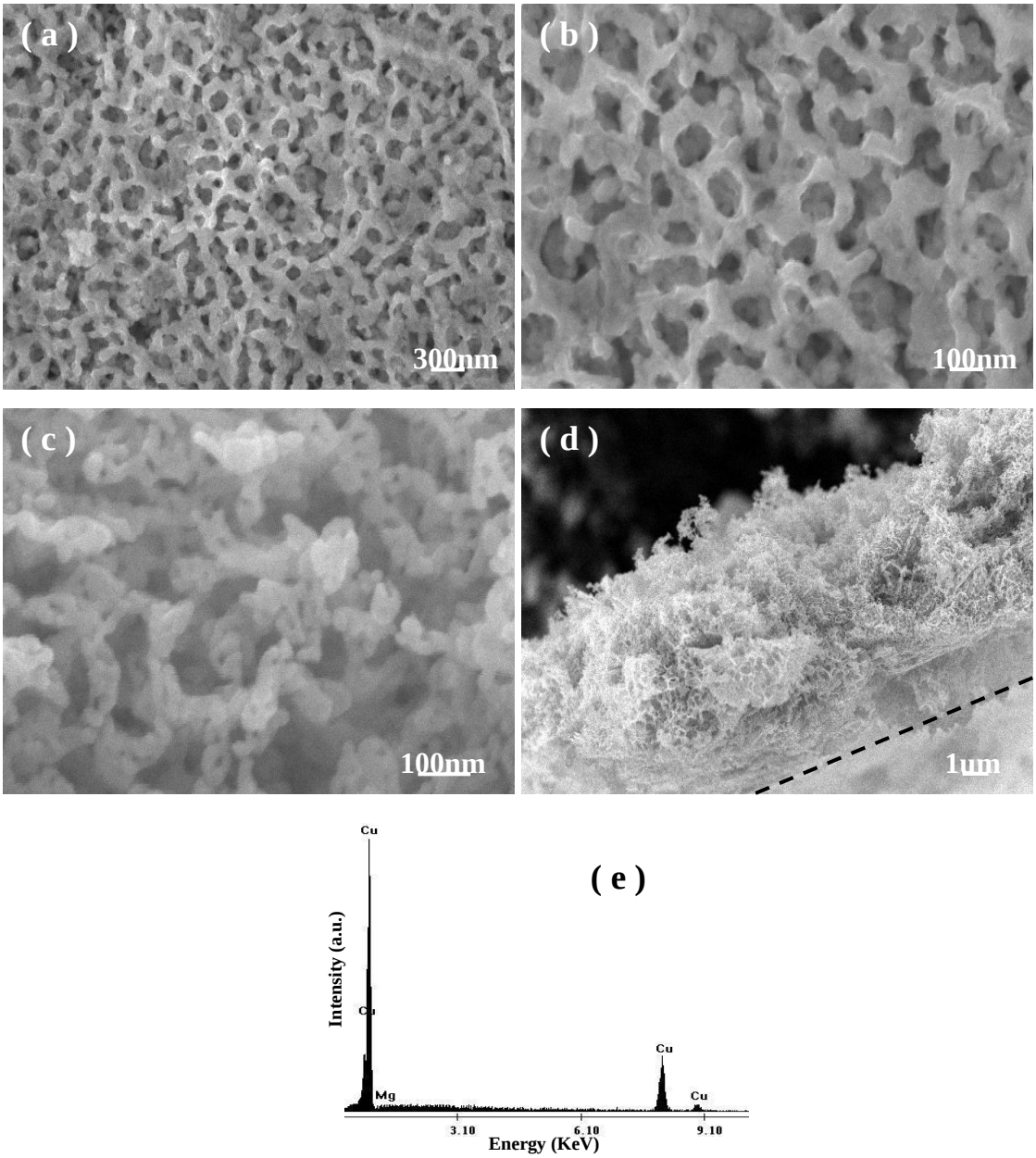

Figure 3. SEM images showing the microstructure of the NPC with hybrid-modal pore size distributions by dealloying in the 1 wt.% HCl solution for 10 min. Parts a and b are the plane views; parts c and d are the section views. Part b shows the plane-view SEM image at a higher magnification; part d shows the entire section-view SEM image at a lower magnification, in which broken line denotes the edge between surface and section. (e) A typical EDX spectrum shows the composition of NPC by dealloying for 10 min. a.u.: arbitrary units.

Thus, the NPC ribbons have bimodal pore size distributions composed of interconnected large-sized pores (~100 nm) with highly porous pore walls (10-20 nm).

Additionally, EDX analysis has been performed on the NPC ribbons and one typical spectrum is shown in part e of Figure 2. Obviously, only Cu can be identified and all of Mg was removed from the Mg 13.5 at.% Cu alloy during dealloying. In contrast, NPG (by dealloying of Ag-Au alloys) normally contains some residual at.% Ag. The residual Ag is expected to be trapped inside the Au ligaments based upon the dealloying mechanism [15,16]. Moreover, the residual Ag can not be removed but asymptotically reaches a limit at exhaustively long etching times (up to 100 h) [15].

Intriguingly, with the dealloying time up to 10 min, the NPC ribbons from the RS Mg 13.5 at.% Cu alloy show that an unique porous structure with hybrid-modal pore size distributions can be obtained and typical SEM images are shown in Figure 3. Comparable with that by dealloying for 5 min, the surface exhibits a uniform network morphology with slightly smaller ligament sizes of 60-80 nm as compared with that of pore dimensions (~100 nm), whereas no obvious porous structure can be observed on the pore walls at a higher magnification (parts a and b of Figure 3). In contrast, the section view of the NPC ribbons shows the large-sized pores continuously penetrate the whole ribbons and the pore walls clearly exhibit an open, bicontinuous interpenetrating ligament-pore structure, indicating that the porous structure in the interior of the NPC ribbons still is characteristic of typical bimodal pore size distributions (parts c and d of Figure 3).

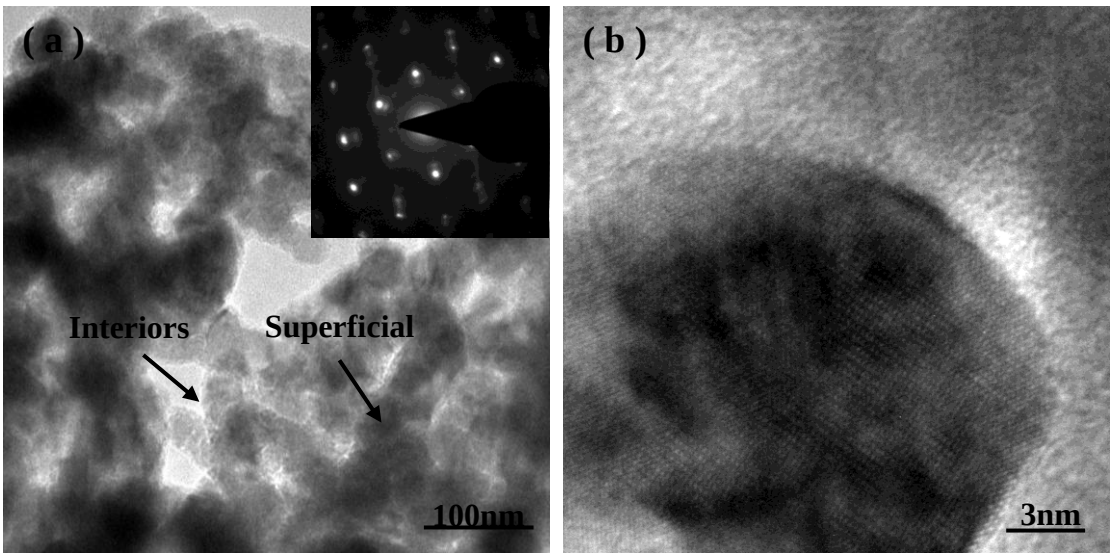

Figure 4. (a) TEM image showing the porous structure with hybrid-modal pore size distributions of the NPC ribbons by dealloying of the Mg 13.5 at.% Cu alloy in the 1 wt.% HCl solution for 10 min. (Inset) SAED pattern corresponding to one ligament in part a. (b) HRTEM image shows lattice fringes extending throughout the whole ligament in the pore walls.

It is worth noting that, with the dealloying time from 5 min up to 10 min, there is little change to the ligament/pore sizes in the interior of NPC ribbons (10-20 nm). EDX analysis has been performed on the NPC ribbons and one typical spectrum shows only Cu can be identified in the as-dealloyed samples upon the dealloying for 10 min (part e of Figure 3). Thus, we herein define the unique NPC featured by a combination of ligament-pore structures with unimodal pore size distributions at superficial layers and those with bimodal pore size distributions in the interior

composed of interconnected large-sized pores with highly porous pore walls as NPC with hybrid-modal pore size distributions. All pores in the ligament-pore structures with unimodal and bimodal pore size distributions are 3D, open and bicontinuous.

TEM observation further verifies the porous structure of NPC ribbons with hybrid-modal pore size distributions upon dealloying in the HCl solution for 10 min and one typical TEM bright-field image is shown in part a of Figure 4. The SAED pattern corresponding to one ligament shows a hexagonal pattern, which is from the f.c.c. Cu [110] zone axis, indicating a single crystalline characteristic of the selected area (inset of Figure 4a). Moreover, lattice fringes extending throughout the whole ligament from the HRTEM image (part b of Figure 4) further verify the single crystal nature of the ligament in the pore walls. It should be noted, however, the present results are essentially different from the established notion that the crystal lattice orientation is retained during dealloying of Ag-Au alloys with the conservation of the grain size of the master alloys [17-20]. For the lattice structure of the resulting NPC is considerably different from that of Mg_2Cu intermetallics in the initial Mg-Cu alloy (Mg_2Cu: face-centered orthorhombic; Cu: f.c.c.).

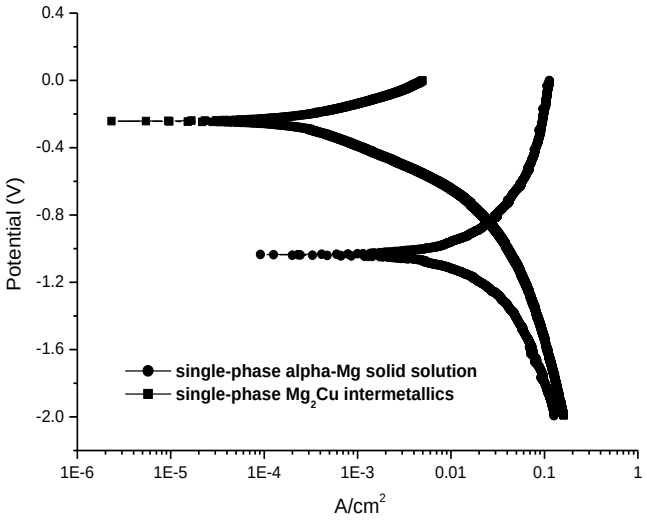

Figure 5. Tafel polarization curves of single-phase α-Mg solid solution and Mg_2Cu intermetallic compound in the HCl solution.

Figure 5 shows Tafel polarization curves of single-phase α-Mg solid solution and Mg_2Cu intermetallic compound in the HCl solution, respectively. It can be found that the difference between free-corrosion potentials of the single-phase α-Mg and Mg_2Cu in the acidic solution is ~793 mV(SCE), which clearly indicates that the α-Mg have a relatively high electrochemical activity compared to the Mg_2Cu in the HCl solution.

The specific surface areas of these porous samples can be evaluated based upon N_2 adsorption/desorption experiments. Figure 6 shows the N_2 adsorption/desorption isotherm for NPC ribbons with hybrid-modal pore size distributions by dealloying of the RS Mg 13.5 at.% Cu alloy in the HCl solution for 10 min. The result shows that the Brunauer-Emmett-Teller (BET) surface area of the appointed sample is much high and has been determined to be 10.6 ± 0.1 m^2 g^{-1}. It is worthwhile

noting that this interesting structural feature endows the NPC ribbons with higher surface area, which is especially beneficial for catalysis and sensing applications.

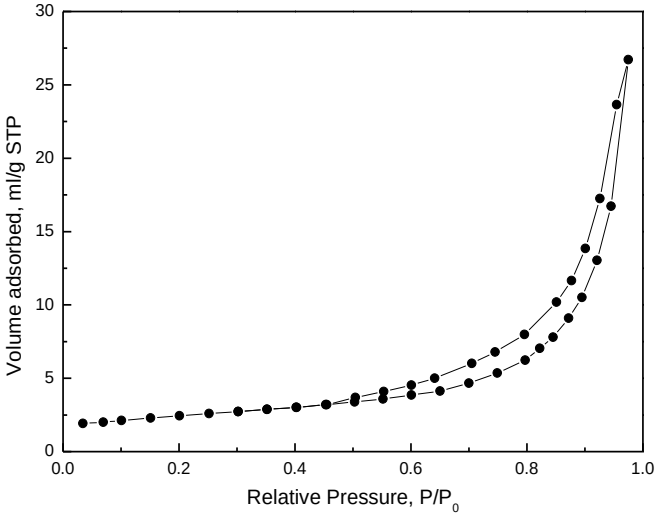

Figure 6. N_2 isotherm at 77 K for the NPC by dealloying of the RS Mg 13.5 at.% Cu alloy in the 1 wt.% HCl solution for 10 min.

It is generally recognized that ideal bicontinuous nanoporous structures are obtained from binary alloy families with a single-phase solid solubility across all compositions by chemical/electrochemical dealloying. The formation mechanism of nanoporous structures during dealloying has been described in the literature [5]. It has been shown that ligaments form as a result of an intrinsic pattern formation during which aggregation of chemically driven noble metal atoms occurs. The process started with selective dissolution of base metal atoms from the outermost alloy surface, leaving behind noble metal atoms that diffused along alloy/solution interfaces and agglomerated into the ligaments. Thus, porosity evolution forms dynamically during dissolution and is not due to one active component simply being excavated out of a binary solid solution alloy [13].

However, if multiple phases exist in an alloy, a more complicated dealloying process will occur. Typically, the present Mg 13.5 at.% Cu alloy is composed of α-Mg and Mg_2Cu phases, in which α-Mg can be entirely dissolved and Mg_2Cu just may be partly corroded. According to the non-equilibrium solidification theory, during the rapid solidification of the Mg 13.5 at.% Cu alloy, eutectics of α-Mg and Mg_2Cu phases can directly nucleate and continually grow from the initial liquid, suppressing the precipitation of primary α-Mg phase due to the fast cooling rate, characteristic of an ideal two-phase bicontinuous microstructure (namely, quasieutectic structure). As indicated in Figure 5, the electrochemical activity of α-Mg is much higher than that of Mg_2Cu. Thus, α-Mg and Mg_2Cu phases existing in the alloys can form corrosion couple cells, with the α-Mg (Mg-rich phase) acting as an anode and preferentially dissolving during dealloying compared to the Mg_2Cu. The preferential dissolution of α-Mg phase forms a large number of tiny paths like a 3D porous network for the penetration of the solution throughout the whole thickness of the ribbons, and the dealloying of α-Mg

facilitates that of Mg_2Cu in which Mg can be selectively preferentially etched. On the other hand, the continuous excavation of the interconnected α-Mg phase from the microstructure during the etching contributes to the formation of the large-sized pores in the resultant NPC, like the case for porous glasses [21], while the dealloying of the Mg_2Cu intermetallics results in the nanoporous structure of the pore walls. Obviously, it is in good agreement with the SEM observations, indicating the microstructure of the NPC strongly depends on the phase distribution of the initial alloy. This is why the NPC ribbons with bimodal pore size distributions composed of interconnected large-sized pores with highly porous pore walls can be obtained as the dealloying time for 5 min.

With the dealloying time up to 10 min, porous structure of the NPC ribbons from the RS Mg 13.5 at.% Cu alloy gradually coarsens through surface diffusion of Cu atoms based upon the Ostwald ripening effects [22]. However, the coarsening rate of the porous structure along the thickness direction of the NPC ribbons is distinctly different, as discussed in detail in the following part.

It was reported that the surface diffusivity in solution of Cu atoms along alloy/solution interfaces is generally of order of 10^{-10} cm^2 s^{-1}, and the adsorption of chloride ion (Cl^-) in HCl solution can greatly enhance the surface diffusion of Cu atoms during the dealloying [23,24]. As far as given dealloying solutions and alloy systems are concerned, surface diffusion of noble metal atoms along alloy/solution interfaces strongly depends upon dealloying solution concentration [5,11,13,25-26], and that is just the adsorbed Cl^- concentration in the present case. It might remarkably modify the enthalpy and entropy of formation of surface moving entities and adsorbed bonds between neighboring sites due to electron transfer reactions [27,28]. Obviously, adsorbed Cl^- concentration at the superficial layers of samples is much higher than that in the interior because nano-scaled channels near the outmost surface severely restrict the transport of ions into the inner space of the structure [29]. Thus, the surface diffusivity of Cu atoms at the superficial layers can be significantly enhanced. These will be further discussed based on the calculations on the surface diffusivity in the following section.

Table 1. The ligament sizes at the superficial layers and in the interiors of the NPC ribbons by dealloying of RS Mg 13.5 at.% Cu alloy in the HCl solution for 10 min, the corresponding surface diffusivities estimated by Eq. (1) [30-31].

Sites in the samples	Interiors	Superficial layers
Dealloying temperature (T, K)	298	298
Dealloying time (t, s)	600	600
Ligament size (d(t), nm)	15±5	70±10
Surface diffusivity (D_S, m^2 s^{-1})	3.55×10^{-19}	1.68×10^{-16}

It has been reported that a maximally unstable spatial period relationship has been predicted for the characteristic length scale (d) of nanoporous metals and surface diffusivity (D_S): $d \propto (D_S/V_0)^{\mu}$, where V_0 is the velocity of a flat alloy surface with no MN atoms accumulated upon it and μ is a constant, suggested to be 1/6 or 1/4 [5,30]. Based on the surface diffusion controlled coarsening mechanism, the D_S values of Cu atoms along alloy/solution interfaces can be estimated by the equation [30-31]:

$D_S = \frac{[d(t)]^4 kT}{32\gamma t\alpha^4}$ (1), where k is the Boltzmann constant (1.3806×10^{-23} J K^{-1}), γ is the surface energy (1.79 J m^{-2}) [32], $d(t)$ is the ligament size at the dealloying time t, α is the lattice parameter of Cu (3.6153×10^{-10} m), and T is the dealloying temperature. According to the ligament sizes at the superficial layers and in the interior of the NPC by dealloying of RS Mg 13.5 at.% Cu alloy in the HCl solution for 10 min, the D_S of Cu atoms at the superficial layers and in the interior was calculated, respectively, as listed in Table 1. It is astonishing that the D_S of Cu atoms at the superficial layers of samples, 1.68×10^{-16} m^2 s^{-1}, is two orders of magnitude greater than that in the interior (3.55×10^{-19} m^2 s^{-1}), indicating the occurrence of substantial coarsening with greater diffusivity at the superficial layers of the NPC ribbons.

Moreover, it should be noted that the coarsening rate of porous structure at the different sites of superficial layers of the NPC ribbons is also remarkably different. Obviously, the nanoporous structure in the pore walls of superficial layers coarsens faster driven by its higher surface energy, thus resulting in the formation of porous structure with unimodal pore size distributions at the superficial layers of the NPC ribbons upon the complete disappearance of nano-scaled pores in the pore walls of superficial layers. On the contrary, as a result of the severe restriction of transport of Cl^- ions, there is little noticeable coarsening occurrence in the interior of NPC ribbons when the dealloying time from 5 min up to 10 min. This is why as the dealloying time increasing to 10 min, the porous structure at the superficial layers of NPC ribbons has changed into that with unimodal pore size distributions, while the porous characteristics with bimodal pore size distributions still exist in the interior.

Based on our present work, it can be proposed that one can employ this simple and effective one-pot strategy to obtain NPMs with hybrid-modal pore size distributions from dual-phase alloys with quasieutectic structures, such as the NPC with hybrid-modal pore size distributions. It will have important implications for further fabricating novel nanoporous materials with more complex structures from multi-phase alloy families. Meanwhile, compared to other methods in the literatures, this strategy possesses evident advantages of simple processing, economy, and is applicable for large-scale synthesis. Additionally, the present work will lay a solid foundation for the promising applications of NPC in lithium ion batteries within the green, new energy industry. Some encouraging test findings have been obtained in our previous work [33-35], the extensive study is in progress.

4. CONCLUSION

We present a simple and effective one-pot approach to synthesize NPC ribbons with hybrid-modal pore size distributions by controlling the surface diffusivity of Cu atoms during chemical dealloying of dual-phase Mg 13.5 at.% Cu alloy with quasieutectic structures in the HCl solution. The as-made NPC ribbons can be featured by a combination of ligament-pore structures with unimodal pore size distributions at superficial layers and those with bimodal pore size distributions in the interior composed of interconnected large-sized pores with highly porous pore walls. All pores in the ligament-pore structures with unimodal and bimodal pore size distributions are 3D, open and bicontinuous. The formation of the unique NPC ribbons can be explained as a consequence of the greater diffusivity of

Cu atoms at the superficial layers induced by the higher absorbed Cl^- concentration. Compared to other methods in the literatures, this approach possesses evident advantages of simple processing, economy, and is applicable for large-scale synthesis. The present work will have important implications for further fabricating novel porous materials with more complex structures from multi-phase alloy families.

ACKNOWLEDGEMENT
We give thanks to financial support by the State Key Basic Research Program of PRC (2007CB936502), the National Natural Science Foundation of China (50574008, 50954005, 51074011), the National 863 Program Project (2006AA03Z230, 2008AA03Z208), the China Postdoctoral Science Foundation Funded Project (2011M500214), and the Basic Research Fund Project of Beihang University (501LJJC2012101001). Also, we are grateful to Prof. T. Zhang and Dr. J.F. Wang for assistance in preparation of the starting alloy ribbons.

References

1. G. C. Bond and D. T. Thompson, *Catal. Rev.,* 41 (1999) 319.
2. T. You, O. Niwa, M. Tomita and S. Hirono, *Anal. Chem.,* 75 (2003) 2080.
3. J. R. Weissmueller, N. Viswanath, D. Kramer, P. Zimmer, R. Wuerschum and H. Gleiter, *Science,* 300 (2003) 312.
4. S. H. Joo, S. J. Choi, K. J. Kwa and Z. Liu, *Nature,* 412 (2001) 169.
5. J. Erlebacher, M. J. Aziz, A. Karma, N. Dimitrov and K. Sieradzki, *Nature,* 410 (2001) 450.
6. K. Sieradzki, N. Dimitrov, D. Movrin, C. McCall, N. Vasiljevic and J. Erlebacher, *J. Electrochem. Soc.,* 149 (2002) B370.
7. W. B. Liu, S. C. Zhang, N. Li, J. W. Zheng, S. S. An and Y. L. Xing, *Int. J. Electrochem. Sci.,* 7 (2012) 2240.
8. M. Stratmann and M. Rohwerder, *Nature,* 410 (2001) 420.
9. Y. Ding and J. Erlebacher, *J. Am. Chem. Soc.,* 125 (2003) 7772.
10. Z. H. Zhang, Y. Wang, Z. Qi, J. K. Lin and X. F. Bian, *J. Phys. Chem. C,* 113 (2009) 1308.
11. Z. H. Zhang, Y. Wang, Z. Qi, W. H. Zhang, J. Y. Qin and J. Frenzel, *J. Phys. Chem. C,* 113 (2009) 12629.
12. W. B. Liu, S. C. Zhang, N. Li, J. W. Zheng and Y. L. Xing, *J. Electrochem. Soc.,* 158 (2011) D611.
13. J. Erlebacher, *J. Electrochem. Soc.,* 151 (2004) C614.
14. W. B. Liu, S. C. Zhang, N. Li, J. W. Zheng, S. S. An and Y. L. Xing, *Int. J. Electrochem. Sci.,* 6 (2011) 5445.
15. M. C. Dixon, T. A. Daniel, M. Hieda, D. M. Smilgies, M. H. W. Chan and D. L. Allara, *Langmuir,* 23 (2007) 2414.
16. K. Sieradzki, R. R. Corderman and K. Shukla, *Phil. Mag. A,* 59 (1989) 713.
17. Y. Ding, Y. J. Kim and J. Erlebacher, *Adv. Mater.,* 16 (2004) 1897.
18. Y. Ding, A. Mathur, M. W. Chen and J. Erlebacher, *Angew. Chem., Int. Ed.,* 44 (2005) 4002.
19. S. Parida, D. Kramer, C. A. Volkert, H. R ö sner, J. Erlebacher and J. Weissm ü ller, *Phys. Rev. Lett.,* 97 (2006) 035504.
20. A. J. Forty and P. Durkin, *Philos. Mag. A,* 42 (1980) 295.
21. D. Enke, F. Janowski and W. Schwieger, *Microporous Mesoporous Mater.,* 60 (2003) 19.
22. A. M. Hodge, J. Biener, J. R. Hayes, P. M. Bythrow, C. A. Volkert and A. V. Hamza, *Acta Mater.,* 55 (2007) 1343.

23. Z. Qi, C. C. Zhao, X. G. Wang, J. K. Lin, W. Shao, Z. H. Zhang and X. F. Bian, *J. Phys. Chem. C*, 113 (2009) 6694.
24. W. B. Liu, S. C. Zhang, N. Li, J. W. Zheng and Y. L. Xing, *J. Electrochem. Soc.*, 157 (2010) D666.
25. W. B. Liu, S. C. Zhang, N. Li, J. W. Zheng and Y. L. Xing, *Microporous Mesoporous Mater.*, 138 (2011) 1.
26. Z. H. Zhang, Y. Wang, Y. Z. Wang, X. G. Wang, Z. Qi, H. Ji and C. C. Zhao, *Scripta Mater.*, 62 (2010) 137.
27. J. M. Dona and J. Gonzalez-Velasco, *Surf. Sci.*, 274 (1992) 205.
28. J. M. Dona and J. Gonzalez-Velasco, *J. Phys. Chem.*, 97 (1993) 4714.
29. H. C. Shin and M. L. Liu, *Chem. Mater.*, 16 (2004) 5461.
30. L. H. Qian and M. W. Chen, *Appl. Phys. Lett.*, 91 (2007) 083105.
31. G. Andreasen, M. Nazzarro, J. Ramirez, R. C. Salvarezza and A. J. Arvia, *J. Electrochem. Soc.*, 143 (1996) 466.
32. W. R. Tyson and W. A. Miller, *Surf. Sci.*, 62 (1977) 267.
33. S. C. Zhang, Y. L. Xing, W. B. Liu and J. W. Zheng, *The 15th International Meeting on Lithium Batteries, IMLB*, J. Electrochem. Soc., Abstract #82, Montréal, Canada, June 27-July 2, 2010.
34. J. W. Zheng, S. C. Zhang, W. B. Liu, Y. L. Xing and Z. J. Du, *J. New Mat. Electrochem. Systems*, 14 (2011) 213.
35. W. B. Liu, S. C. Zhang, J. W. Zheng and Y. L. Xing, *The 4th international conference on advanced lithium batteries for automobile application, ABAA-4*, Tianjin Institute of Power Sources & China Industrial Association of Power Sources, Abstract #108, Beijing, China, September 21-23, 2011.